Mechanistic modelling of water partitioning behaviour in hydrocyclone

Chandranath Banerjee [a], Eric Climent [b], Arun Kumar Majumder [a,*]

[a] Department of Mining Engineering, Indian Institute of Technology Kharagpur, Kharagpur 721302, India
[b] Institute of Fluids Mechanics, UMR 5502 CNRS-INPT-UPS Allée Pr. Camille Soula, 31400 Toulouse, France

HIGHLIGHTS

- Phenomenological features of swirl flow hydrodynamics in a hydrocyclone.
- Quantitative description of water transport mechanism in hydrocyclone.
- Effect of *G* force distribution on hydrocyclone flow split.
- A new model for the water split is proposed.
- Experiments, simulations and model accuracy are discussed.

ABSTRACT

A new mechanistic model on water split behaviour in a hydrocyclone has been developed based on the convoluted hydrodynamics of swirling flows in a confined environment. A comprehensive study has been accomplished on the genesis and subsequent distribution of *G* force based on the characterization of internal flow features of a 2 in hydrocyclone through computational fluid dynamics (CFD) approach. The difference between the magnitude of *G* force in cylindrical and spigot regions is taken into account as a new hydrodynamic parameter to compute the water split behaviour. Specifically, our analysis reveals a semi-empirical relationship between the water split with *G* force difference (ΔG), the vortex finder diameter (D_{vf}) and the spigot diameter (D_{sp}). The developed model is validated against experimental data and show good prediction accuracy. Unique aspect of the developed empirical model is that the underlying mechanism of incipient flow peculiarity is implicitly accounted to rummage the separation characteristics in a quantifiable manner. In addition to rationalize the flow split behaviour of hydrocyclones, this new hydrodynamic indicator seems promising to be used as a scale-up parameter in envisaging the separation performance for a given application.

Keywords:
Water split
Hydrodynamics
G force difference
CFD
Hydrocyclone

1. Introduction

Hydrocyclones have vast engineering applications in various sectors like mining, chemical, petroleum, nuclear, environment, food processing, etc. Although the popularity of hydrocyclone is primarily attributable to its apparently simple design and operational features, imprecise particle separation remains a major drawback. In reality, the particle separation mechanism in a hydrocyclone is very complicated due to its cylindro-conical geometry and the presence of strong swirling flow (Ovalle and Concha, 2005; Gupta et al., 2008; Davailles et al., 2012; Swain and Mohanty, 2013; Banerjee et al., 2015) which results into turbulence. Probably due to this reason, a tailor-made design of hydrocyclone for a specific application is still non-existent. The solutions to those aforementioned problems associated with hydrocyclones can only be provided once the physics of particle separation in a centrifugal flow field is properly understood. Since from the modelling point of view the intricate details of particle and fluid flow behaviour inside a hydrocyclone is a complex aspect to realize, many attempts have been made to develop empirical models to assist industry professionals and designers (Lynch and Rao, 1975; Plitt, 1976; Chen et al., 2000; Coelho and Medronho, 2001; Nageswararao et al., 2004; Narasimha et al., 2014).

However, as the models are empirical, the coefficients against each variable have to be determined experimentally when either the material to be processed or the basic design of hydrocyclone is changed even marginally. As this is impractical in many situations the performance of industrial scale hydrocyclones is mostly

* Corresponding author.
E-mail address: akm@mining.iitkgp.ernet.in (A.K. Majumder).

http://dx.doi.org/10.1016/j.ces.2016.06.037

Nomenclature

D_{sp}	spigot diameter (mm)
D_{vf}	vortex finder diameter (mm)
D_i	feed inlet diameter (mm)
D_c	hydrocyclone cylindrical diameter (mm)
R_c	hydrocyclone radius (mm)
d_c	hydrocyclone diameter at any location (mm)
r_t	cutoff radius separating the forced and the free vortex
R_t	normalized cutoff radius ($= r_t/R_c$) (dimensionless)
R	normalized radial location ($= r/R_c$) (dimensionless)
r	any radial location (mm)
r_m	radial location of maximum tangential velocity (mm)
Q_{of}	water mass flow rate in overflow (kg/s)
Q_u	water mass flow rate in underflow (kg/s)
S	water split ($= Q_u/Q_{of}$) (dimensionless)
P	static pressure (kPa)
P_{in}	inlet pressure (kPa)
z	axial distance from the top wall (mm)
L_s	mixing length for subgrid scale model (m)
$\overline{u}_i$	filtered velocity (m s^{-1})
μ_t	sub-grid scale eddy viscosity (kg m^{-1} s^{-1})
τ_{ij}^{sgs}	sub-grid scale stress tensor (N/m^2)
$\overline{S}_{ij}$	mean strain rate (s^{-1})
ρ	density (kg/m^3)
Δ	filter width (m)
ω	angular velocity (s^{-1})
Γ_α	vortex circulation (m s^{-1})
u	axial velocity (m^{-1})
u_θ	tangential velocity (m^{-1})
$u_{\theta max}$	maximum tangential velocity (m^{-1})
A_i	feed inlet area (mm^2)
Q_i	feed inlet volumetric flow rate (m^3 s^{-1})
ΔG	G force differential (dimensionless)
V_i	feed inlet velocity (m s^{-1})

compromised. By the advent of sophisticated measurement techniques like laser Doppler anemometry (LDA), laser Doppler velocimetry (LDV), particle image velocimetry (PIV), etc. several studies (Kelsall, 1952; Knowles et al., 1973; Dabir and Petty, 1984; Hsieh and Rajamani, 1991; Fisher and Flack, 2002; Lim et al., 2010; Zhen-Bo et al., 2011) attempt to gain fundamental insight of intricate flow features. Besides these experimental studies, literature (Slack et al., 2000; Brennan, 2006; Delgadillo and Rajamani, 2007; Wang and Yu, 2008; Delgadillo and Rajamani, 2009; Karimi et al., 2012; Hwang et al., 2013; Ghodrat et al., 2014; Banerjee et al., 2015) on the numerical modelling approaches to quantify the fluid–particle flow pattern inside a hydrocyclone are also available. While the other class of works aims at analysing convoluted hydrodynamics of the prevailing flow field so as to unveil the phenomenological features leading towards novel design modifications (Mainza et al., 2006; Delgadillo and Rajamani, 2007; Wang and Yu, 2008; Hwang et al., 2012, 2013; Ghodrat et al., 2014). Nevertheless, the accrued industrial benefits are still marginal although the fundamental knowledge domain in this area has been expanded considerably. However, it is essential to develop industrial friendly mathematical models based on those accrued knowledge to overcome the limitations of hydrocyclone as stated above.

We believe that in-depth understanding of the physics of water motion inside a hydrocyclone is a pre-requisite towards this end, as the particles are basically transported through water. Over the past few decades, several models (Moder and Dahlstrom, 1952; Yoshioka and Hotta, 1955; Abbot, 1962; Bradly, 1965; Plitt et al., 1990; Shah et al., 2006; Narasimha et al., 2014; Banerjee et al., 2015) have been proposed to compute water split in classifying cyclones. The aforementioned models are, however, far from being adequate to address various intricate issues of complex hydrodynamic features. In sharp contrast to the existing concepts of modelling on cyclone classification performance, present study provides a mechanistic model to predict water split behaviour of a hydrocyclone based on understanding phenomenological aspects of swirling flow through numerical simulation.

2. Numerical simulation

Pericleous et al. (1984) were possibly the first to report numerical simulation results on vortex formation and the velocity distribution of fluid flow behaviour inside a classifying hydrocyclone. As the accuracy of any such numerical simulation is dependent principally on appropriate turbulence modelling, over time a number of turbulence models have been used to capture the internal hydrodynamics prevailing inside a particular hydrocyclone. Numerous attempts have been made to determine the complex flow pattern using various commercially available computational fluid dynamics (CFD) tools which allow the flexibility in testing various turbulence models. Many authors (Brennan, 2006; Narasimha et al., 2006; Delgadillo and Rajamani, 2007, 2009; Lim et al., 2010; Karimi et al., 2012; Banerjee et al., 2015) have recommended that LES is probably the most appropriate turbulence model to capture all the unsteady aspects of hydrocyclone flow structure because the simulation technique preserves the unsteady nature of the 3D large-scale structures of the flow. Therefore, in the present study the LES approach has been attempted first to test its applicability in validating the water partitioning data generated in a 2 in (50.8 mm) diameter cyclone often used for industrial purposes.

2.1. Fundamental of LES-brief overview

Fundamentally, LES has been developed to take advantage of the Kolmogorov (1941) theory of self-similarity which states that the large eddies of the flow are dependent on geometry while the smaller scales are more universal and are responsible for viscous dissipation. Therefore, it allows one to explicitly resolve the large eddies with a set of equations and implicitly account for the small scale eddies by using a sub-grid scale (SGS) model. LES preserves the time dependent and 3D nature of the large scales of the turbulent flow. As the principal operation in LES is based on low-pass filtering, the governing equations are thus transformed and the resultant solution is a filtered velocity field.

2.2. Governing equations

In LES technique, the following set of equations are solved for mass and momentum balance:

$$\frac{\delta(\rho)}{\delta t} + \frac{\delta(\rho \overline{u}_j)}{\delta x_j} = 0, \quad \text{continuity} \tag{1}$$

$$\frac{\delta(\rho\overline{u}_j)}{\delta t}+\frac{\delta(\rho\overline{u}_i\overline{u}_j)}{\delta x_j}=-\frac{1}{\rho}\frac{\delta\overline{p}}{\delta x_i}+\frac{\delta}{\delta x_j}\left(\mu\frac{\delta\overline{u}_i}{\delta x_j}\right)+\frac{\delta(\tau_{ij}^{sgs})}{\delta x_j}+g_i,\quad \text{momentum} \tag{2}$$

For the present study, the fluid is homogeneous with constant density and flow is considered to be incompressible. Here the quantities with overbar denote the filtered quantities; this can be defined for any variable ϕ as

$$\overline{\phi}(\mathbf{x})=\int_{\Omega}\phi(\mathbf{x}')F(\mathbf{x},\mathbf{x}')d\mathbf{x}' \tag{3}$$

where $F(\mathbf{x},\mathbf{x}')$ is the filtering kernel defined within the domain $\mathbf{x}'\in\Omega$. For computational purpose one can define

$$F(\mathbf{x},\mathbf{x}')=\begin{cases}\dfrac{1}{\Delta V}, & \mathbf{x}'\in\Omega\\ 0, & \text{otherwise}\end{cases} \tag{4}$$

where ΔV is the volume of the computational cell (the filtered flow will be resolved on the mesh grid). In the momentum equations

$$\tau_{ij}=\mu\left(\frac{\partial\overline{u}_i}{\partial x_j}+\frac{\partial\overline{u}_j}{\partial x_i}\right) \tag{5}$$

τ_{ij}^{sgs} denotes the deviatoric stress tensor of hydrodynamic component whereas

$$\tau_{ij}^{sgs}=\overline{u_iu_j}-\overline{u}_i\overline{u}_j \tag{6}$$

τ_{ij}^{sgs} is defined as subgrid-scale-stress tensor. Like Reynolds-averaged Navier–Stokes (RANS) equations, τ_{ij}^{sgs} endorses a closure problem, which can be modelled by employing Boussinesq hypothesis of the form

$$\tau_{ij}^{sgs}=\frac{1}{3}\tau_{kk}^{sgs}-\mu_t\left(\frac{d\overline{u}_i}{dx_j}+\frac{d\overline{u}_j}{dx_i}\right) \tag{7}$$

where the turbulent viscosity μ_t can be estimated by several methods proposed in literature, such as Smagorinsky–Lilly model (SLM), dynamic Smagorinsky–Lilly model, wall-adapting local eddy-viscosity model (WALE), dynamic kinetic energy subgrid-scale model to name a few. All the above mentioned models are available within the commercially available finite volume solver platform FLUENT©. The simplest subgrid-scale model is the Smagorinsky–Lilly model. This model proposes that the subgrid-scale eddy viscosity is related to the local average grid spacing and the filtered strain rate:

$$\mu_t=L_s^2\sqrt{\overline{S_{ij}}\overline{S_{ij}}} \tag{8}$$

where $\overline{S_{ij}}$ is the filtered strain rate and L_s is the length-scale for the sub-grid scale which is given by $C_s\Delta^{1/3}$, where Δ is the computational cell volume. The constant C_s in Fluent is equal to 0.1.

In the centre of hydrocyclones, the strong reduction of pressure due to swirling flows yields the formation of an air core. However, the hydrodynamic modelling of multiphase flow in turbulent swirl flows is a non-trivial computational challenge. Subgrid scale modelling of interface deformation due to turbulence is still an open issue and although both options might be selected simultaneously in commercial CFD softwares there is no validation of such a use on benchmark two-phase flows. Due to the inherent limitation of coupling between turbulent models and multiphase models, many studies have already been reported on hydrocyclone flow field and performance evaluation through CFD modelling approach without simulating the air core features (Gupta et al., 2008; Zhen-Bo et al., 2011; Karimi et al., 2012; Zhu et al., 2012; Murthy and Bhaskar, 2012; Davailles et al., 2012; Hwang et al., 2013; Swain and Mohanty, 2013; Banerjee et al., 2015), while some authors quantified the hydrocyclone flow field from another viewpoint by considering air core as a hollow tube (Chu et al., 2004; Sripriya et al., 2007; Evans et al., 2008). From their results, no discrepancy is observed between the predicted velocity profile and experimental observation reported in existing literature.

2.3. Geometry and mesh

The main body of the cyclone under consideration consists of a cylindrical section with 50.8 mm diameter and 166 mm height as shown in Fig. 1(a). The spigot diameter is variable in size with openings corresponding to 4.5 mm and 6.4 mm with an included angle of 7° suitably maintained by adjusting the height of the conical portion. Vortex finders with two different diameters of 14 mm and 11 mm have also been selected for the study. A rectangular feed inlet opening with dimensions 9 mm × 6 mm is connected tangentially to the main cylindrical body at a height of 20 mm below the top surface. Studies were carried out under the above geometries by changing the inlet feed water pressure. All hydrocyclone details on the design and geometry used for the experimental as well as CFD simulation purposes are presented in Table 1.

As LES is intrinsically a 3D dynamic simulation, a three dimensional body fitted structured grid was, therefore, generated in Gambit. An overall orientation of the grid for the given hydrocyclone geometry is shown in Fig. 1(b). Boundary layer mesh adjacent to the wall region was generated to keep the wall y^+ value within the logarithmic law layer $(30 < y^+ < 300)$ to resolve near-wall turbulent features accurately. For the present study the grid spacing $(\Delta s/R_c)$ varies from 0.1385 in the bulk to 0.001968 near to the wall. It is well known that the accuracy of any numerical simulation depends much on optimum grid densities and this optimum grid density is selected based on the value above which numerical solution will remain unaltered. Sometimes, however, computational time requirement also plays a dominant role in deciding this optimum mesh density. As the focus of the present research was to understand the inherent flow split mechanism, grid resolution study was carried out first with four different mesh densities of 245,000, 415,000, 550,000 and 981,000.

The tangential velocity distributions as a function of radial distance from the central axis of the hydrocyclone at a vertical distance of 120 mm from the roof top at the afore mentioned four mesh densities are shown in Fig. 2. It is evident from this figure that the velocity patterns at different mesh densities are mostly overlapping with each other. However, to ensure reliability the mesh density of 550,000 has been chosen for the entire study. Eqs. (1)–(8) are solved using inlet feed pressure as a boundary condition. As the hydrocyclone is a static vessel, no slip wall boundary conditions were used on the zones affected by the cyclone walls. To ensure statistical steady flow after the transient evolution, total simulation time was adopted for 10 s corresponding to 20,000 time steps. The tolerance limit of the residuals for continuity and velocity was kept in the range of 10^{-4}. To verify the validity of the adopted numerical modelling scheme, the water split at various conditions mentioned in Table 1 were measured experimentally and compared with the simulation data as obtained from LES model. The experimental procedure and the data validation are presented and discussed below.

2.4. Numerical model validation

For experimental data generation, a closed circuit test rig composed of a pump and sump assembly housing a hydrocyclone of 50.8 mm diameter was used. Fig. 3 represents the demonstrative sketch of the experimental test rig. At each operating condition as mentioned in Table 1, water flow rates through overflow and underflow were measured by collecting timed samples at an

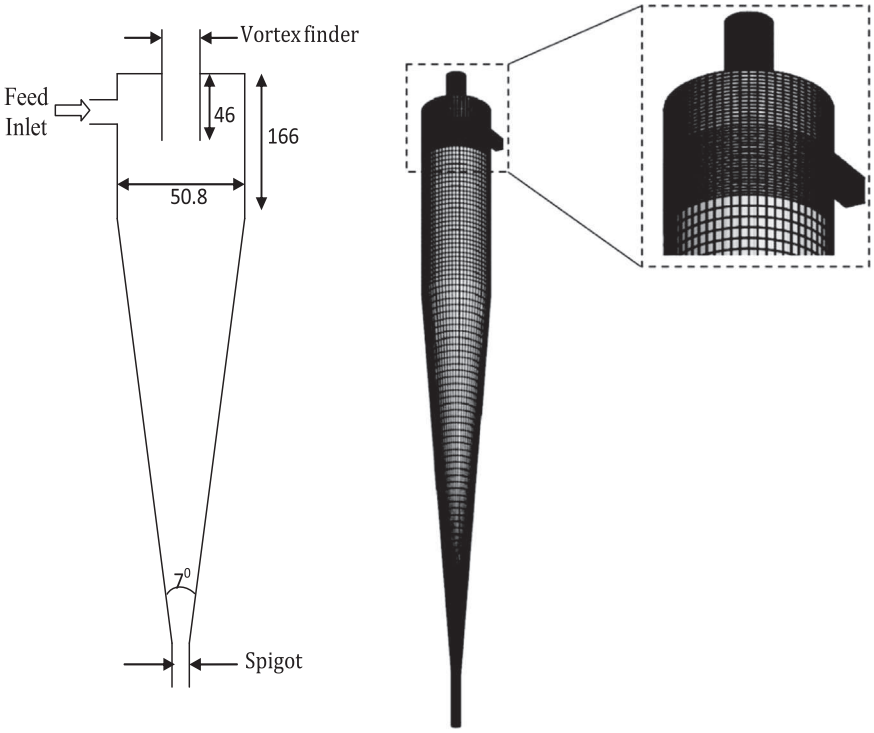

Fig. 1. Schematic diagram of (a) the geometry of hydrocyclone used for the present study (all units are in mm) and (b) mesh structure used for hydrocyclone simulations.

Table 1
Data set used for numerical model validation.

Dimensions	HC-1	HC-2	HC-3
D_c (mm)	50.8	50.8	50.8
D_{vf} (mm)	14	14	11
D_{sp} (mm)	6.4	4.5	4.5
Inlet area (mm^2)	9 × 6	9 × 6	9 × 6
Cone angle	7°	7°	7°
P_{in} (kPa)	68.95, 206.84 344.74	68.95, 206.84 344.74	68.95, 206.84 344.74

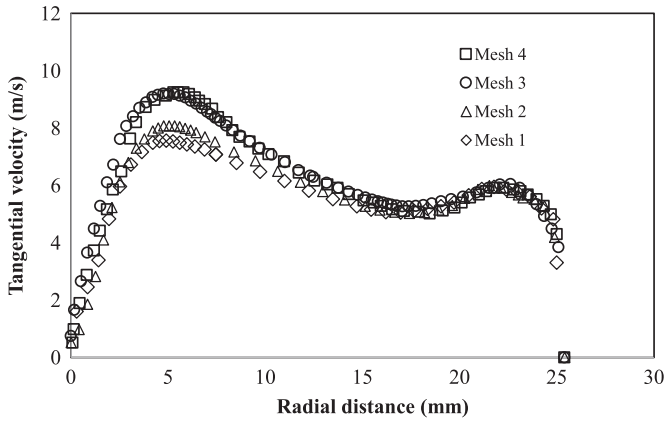

Fig. 2. Grid resolution. Mesh 1 = 245,000; Mesh 2 = 415,000; Mesh 3 = 550,000 and Mesh 4 = 981,000.

interval of 10 s. Percent overflow data with respect to feed flow rate were then calculated from the reconstituted feed thus generated. Each experiment was repeated three times to calculate the standard deviations at 95% confidence interval.

One can obtain steady flows from the overflow and the underflow, for fixed operating conditions (specifically the inlet

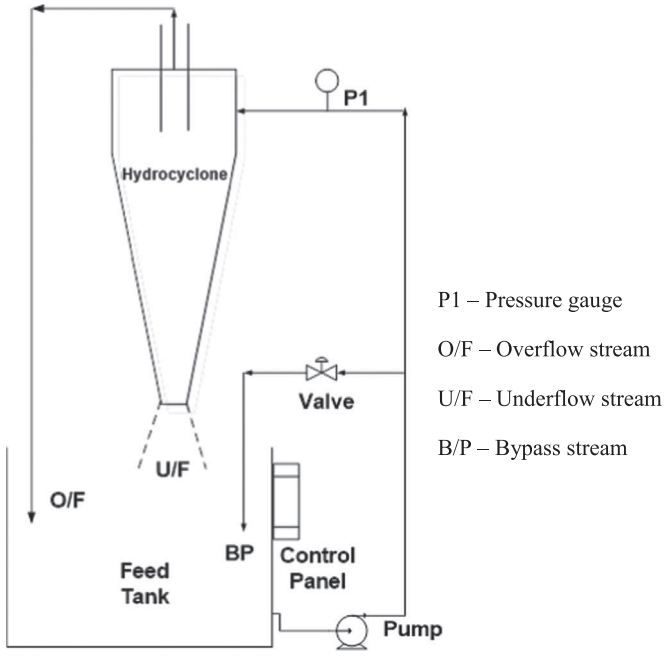

Fig. 3. Schematic of the experimental test rig.

pressure). The overflow flow rate with time, as obtained from present simulation is shown in Fig. 4. Here a typical case from the set with D_{vf} = 14 mm and D_{sp} = 4.5 mm has been shown. The figure shows that after transient time, simulation provides nearly steady flows through the overflow. While presenting the results, the data obtained during this nearly steady operation regime are considered.

Fig. 5 illustrates the computed root-mean-square (rms) values of the tangential velocity at each time step. The instantaneous velocity at each time step was recorded for 500 iterations, from

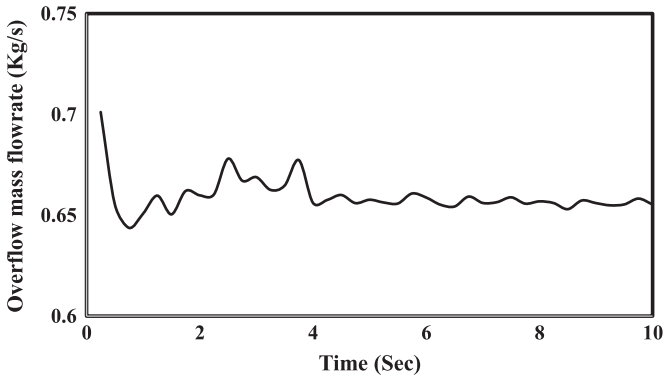

Fig. 4. Time variation of the mass flow rate reported to overflow, as obtained from the present simulation.

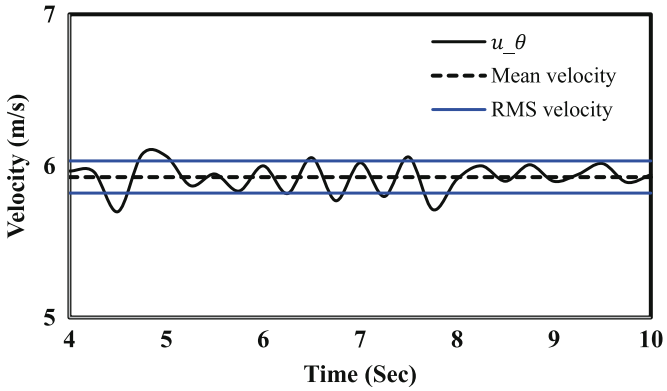

Fig. 5. Temporal evolution of the tangential velocity at 120 mm from cyclone roof. Mean and rms are shown with dashed and blue lines, respectively. (For interpretation of the references to colour in this figure caption, the reader is referred to the web version of this paper.)

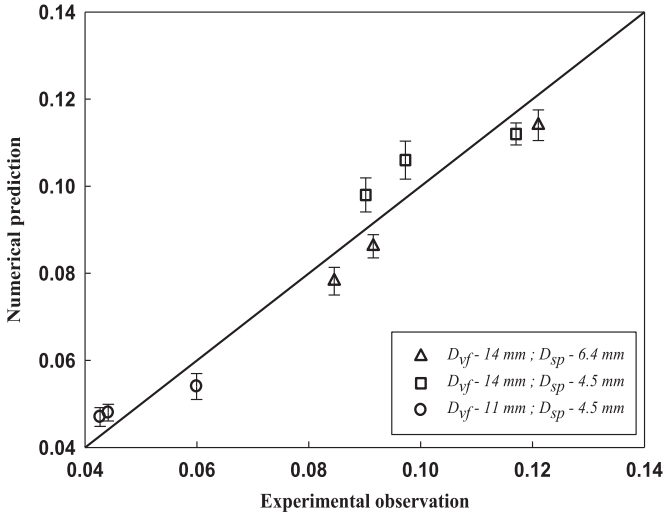

Fig. 6. Comparison between the experimental and numerical prediction of water split.

which rms deviation velocities along with mean velocity were calculated. The deviation of the instantaneous velocity with respect to mean denotes the resultant turbulent fluctuations in the prevailing swirling flow which take place inside the hydrocyclone. The comparative plot between the experimental data and the numerical predicted data is shown in Fig. 6. From Fig. 6, it is evident that numerically predicted data are in good agreement with the experimental data with maximum error of 9%.

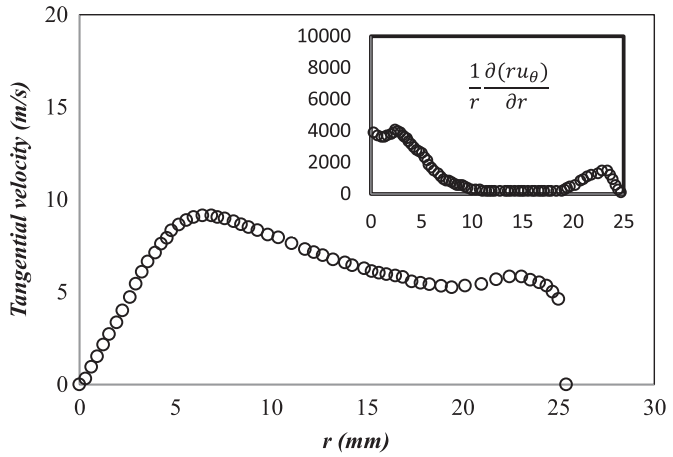

Fig. 7. Radial distribution of the tangential velocity as obtained from the present simulation. The inset shows the corresponding distribution of $\frac{1}{r}\frac{\partial}{\partial r}(ru_\theta)$.

2.5. Numerical data analysis

As the present single phase simulations have been validated, we extended the present simulation setup in capturing the gross hydrodynamic features of a 2-in hydrocyclone. Our principle target of this analysis was to apprehend the intricate details of hydrodynamics of a hydrocyclone with an ultimate aim to understand the variations of G force distribution responsible for flow splits. Close scrutiny of the inherent flow field inside a hydrocyclone reveals the existence of a force-vortex flow near the central region and free-vortex flow otherwise (Ovalle and Concha, 2005; Wang and Yu, 2008; Yao and Fang, 2012; Banerjee et al., 2015). This composite vortex-flow is the reminiscent of a Rankine vortex flow, studied, quite extensively, however, in other contexts (Kreith and Sonju, 1965; Julien, 1986; Darmofal et al., 2001; Yao and Fang, 2012). The tangential velocity component is considered to be the most dominant velocity component in the hydrocyclone literature (Hsieh and Rajamani, 1991; Brennan, 2006; Delgadillo and Rajamani, 2007; Wang et al., 2007; Wang and Yu, 2008; Delgadillo and Rajamani, 2009) and it is primarily responsible for driving out the fluid through overflow. Fig. 7 presents the radial distribution of the tangential velocity profile at the axial location $z = 120$ mm measured from the roof of the hydrocyclone.

However, without any loss of generality, it can be expected that a composite vortex type flow profile comprises of free and forced vortex zone, as specifically emphasized in the inset of Fig. 7. Specifically, near the central region (the region close to $r=0$), a high magnitude of $\frac{1}{r}\frac{\partial}{\partial r}(ru_\theta)$ signifying the presence of strong forced vortex zone. Subsequently, the magnitude of $\frac{1}{r}\frac{\partial}{\partial r}(ru_\theta)$ reduces to very low value towards the wall, this feature is the reminiscent of a free vortex zone. Typical tangential velocity profiles at $z = 60$, 120, 180 and 240 mm are shown in Fig. 8, as obtained from the present simulations. From the figures it seems that tangential velocity will not change significantly in the cylindrical section but as it moves towards conical section its magnitude at a specific radial position decreases which is possible due to the successive decay of the swirling intensity.

Subsequently in Fig. 9(a) the variation of force profiles at identical location (as shown in Fig. 8) has been plotted. The contour plot of G force inside the cyclone has been presented in Fig. 9 (b). G force is defined as the ratio of the centrifugal force to the gravitational force $G = u_\theta^2/rg$. From Fig. 8 it is also observed that within the vortex core region the G force reaches its maximum value. It is then gradually decreasing with increasing radial distance from the central axis and reaches zero near the wall. From Fig. 9(a) it appears that G_{max} (corresponds to the maximum value

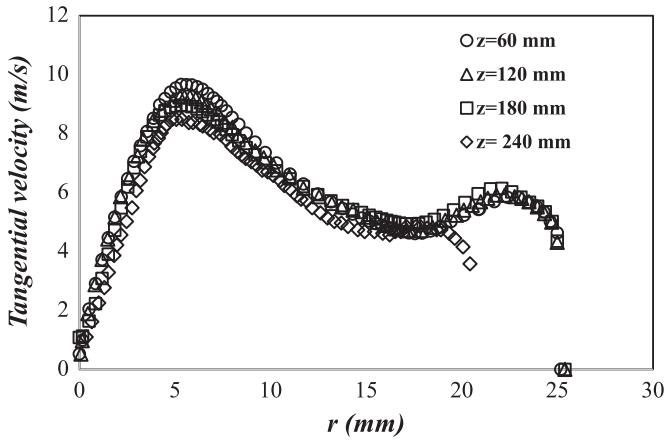

Fig. 8. Tangential velocity profiles in hydrocyclone.

of G force profile) remains almost constant in the cylindrical section but there is a significant drop in G_{max} value in the conical part. Fig. 9(b) represents the contour plot of G force distribution for a given cyclone as obtained from present simulation. From the G force contour, one can observe that near the forced vortex region, G reaches high value. From the present observations, it seems rational to consider the variation in G force between cylindrical and conical section has a significant influence in deciding the flow split phenomenon under the hydrodynamic environment of swirl flow inside a hydrocyclone.

It is believed that the inner vortex (which corresponds to low pressure region is precisely the location of air core) in a hydrocyclone originates near the spigot region and exits through the vortex finder at a high velocity. It is well known that due to the pressure drop between the spigot and vortex finder region this air core forms having an upward flowing direction. Possibly when this air core moves at a high velocity in an upward direction from the spigot region, local drag is formed which carries water (available in the vicinity) in an upward direction too. Therefore, to further analyse this intrinsic fluid flow behaviour, the fluid velocity vectors at various planes along the vertical central axis at each simulated condition have been obtained. A snapshot at a given operating condition of this velocity vector near the vortex finder zone is shown in Fig. 10(a). It may be observed that there exists a flow reversal. This flow reversal probably happens due to the formation of two rotating spirals in opposite directions. At the boundary between these two spirals the flow is having no velocity, which may be because of the shear.

From the tangential velocity components presented in Fig. 8 at each location in the radial as well as axial directions, it is clear that pressure drop exists in the radial direction. Radial pressure drop causes a part of the flow to move along the core region and join the fluid moving in the upwards direction due to axial velocity. As the fluid moves upward its velocity starts accelerating due to the additional flow because of radial pressure drop and the axial velocity, therefore, reaches its maximum value just before entering the vortex finder. This is probably the governing factor for the flow split mechanism inside the hydrocyclone. Nevertheless, the fundamental insight gained from the numerical analysis of a hydrocyclone provides sufficient rationale against the observed phenomenological features. However, this analysis is still limited to the level of physical arguments and comparative descriptions. Translation of those concepts to meet engineering requirements (namely design, operation) is rather obscure without invoking any empiricism. An attempt has, therefore, been made to use the afore-mentioned information generated to develop a new and simple model to predict the water partitioning behaviour inside a hydrocyclone in the following fashion.

3. New concept

The flow field inside a hydrocyclone resembles the Rankine vortex flow which implies that the tangential velocity is composed of free and forced vortex contributions. The tangential velocity distribution of a Rankine vortex flow at a given axial location can be obtained by the following equation (Yao and Fang, 2012):

$$u_\theta = u_{\theta max}\begin{cases}\dfrac{R}{R_t}, & R < R_t \quad \text{(forced vortex)}\\ \dfrac{R_t}{R}\left(\dfrac{1-R}{1-R_t}\right), & R \geq R_t \quad \text{(free vortex)}\end{cases} \tag{9}$$

The matching region between free and forced vortex component denotes the zone of maximum tangential velocity $u_{\theta max}$. It is imperative to note that the hydrocyclone performance is essentially governed by the prevailing swirling flow inside the cylindrical section. In this context maximum magnitude of tangential velocity at the chosen axial location of the cylindrical section can be obtained from eigen value problem (Yao and Fang, 2012). Therefore,

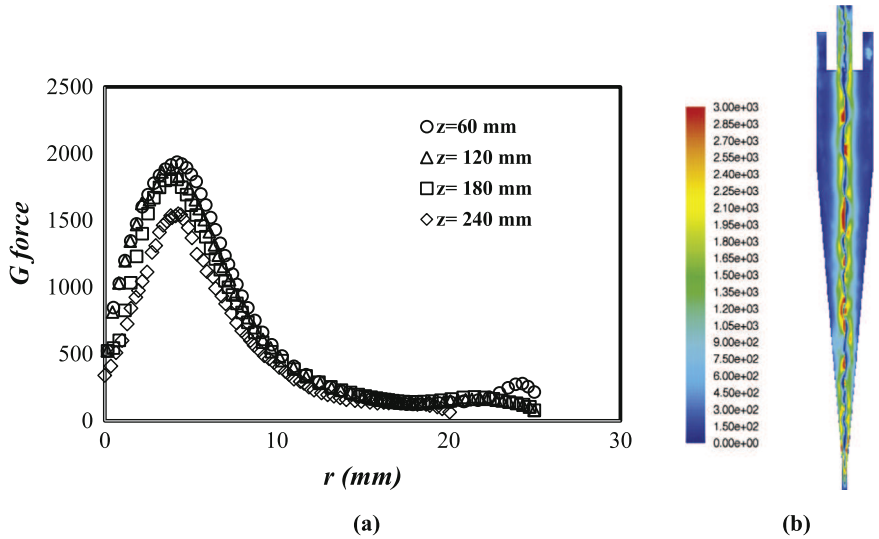

(a) (b)

Fig. 9. (a) G force distribution at different axial heights and (b) contour plot of G force distribution.

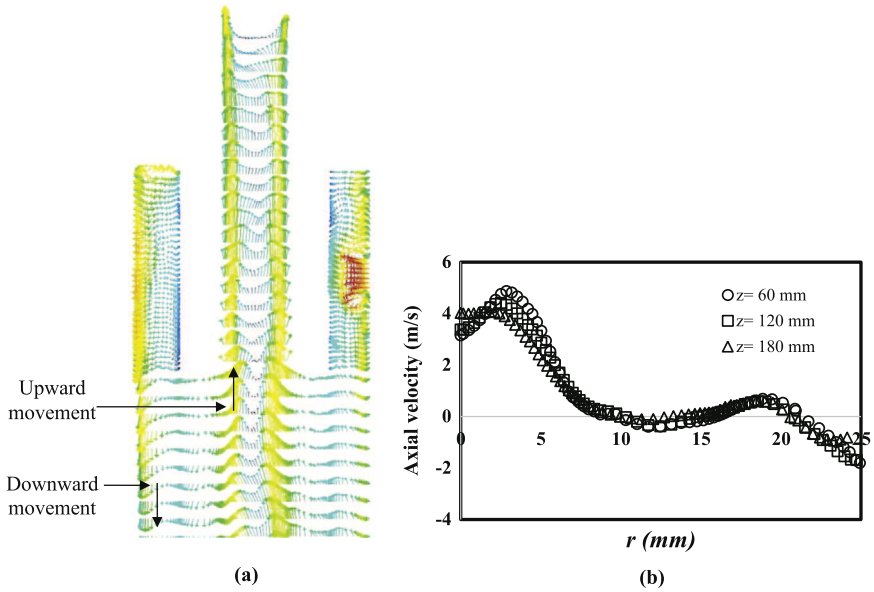

Fig. 10. (a) Fluid velocity vector near the vortex finder and (b) axial velocity profile at different z locations.

in this paper, from the perspective of theoretical analysis, we are restricting our attention inside the cylindrical section only to bring out the essential physics of Rankine vortex flow. In case of water, the fluid can easily be considered as incompressible with constant density and with the approximation that the radial velocity is negligible then the radial momentum equation reduces for steady flow:

$$\frac{u_\theta^2}{r} = \frac{1}{\rho}\frac{\delta p}{\delta r} \tag{10}$$

An expression for the static pressure distribution (Darmofal et al., 2001) can be quantified as

$$p(r, z) - p_o = \rho\omega^2\frac{r^2}{2}, \quad \text{forced vortex} \tag{11}$$

$$p(r, z) - p_\infty = -\frac{\rho\Gamma_\alpha^2}{8\pi^2 r^2}, \quad \text{free vortex} \tag{12}$$

The schematic representation of tangential velocity and static pressure distribution in a Rankine vortex flow is represented in Fig. 11. The pressure variation in the forced vortex region is generated due to the radial variations of the tangential velocity. A typical profile of $u_\theta/u_{\theta max}$ at $z/R_c = 0.1$, 1, 10 and 100 as obtained from theoretical analysis is shown in Fig. 12(a). Subsequently, radial variations of $u_\theta/u_{\theta max}$ for $R_t = 0.1$, 0.15 and 0.2 at a given axial location are shown in Fig. 12(b). Following the lead, we compare the theoretical prediction against the numerical results of $u_\theta/u_{\theta max}$ at a specific z location (z – 120 mm). From the comparison it appears that the present theoretical trend provides at least a rationalization against the LES estimation. From Fig. 12 it also appears that both z and R_t play significant role in deciding $u_{\theta max}$. With the reference of Fig. 12(a), it is worth mentioning that kinetic energy dissipates with the position which results a significant decay in swirl flow. But this phenomenon is very much obvious when the length of the cylindrical section is much longer. In general, the variation of tangential velocity from cyclone roof to conical section is very minimal (Hsieh and Rajamani, 1991; Brennan, 2006; Narasimha et al., 2006; Delgadillo and Rajamani, 2009). Therefore we can argue that the R_t plays more significant role in deciding the magnitude of G force. Since the inner vortex which is mainly occupied by air core behaves like a solid body (Ovalle and Concha, 2005) and therefore the transport of water and also slurry through the overflow stream are mainly controlled by the induced shear created by the inner vortex. In connection to the above theoretical interpretation on Rankine vortex flow, one can appreciate that a radial pressure drop essentially takes place both in cylindrical section and the conical section as well due to the prevailing swirling flow. However, forced vortex plays a major role in flow-

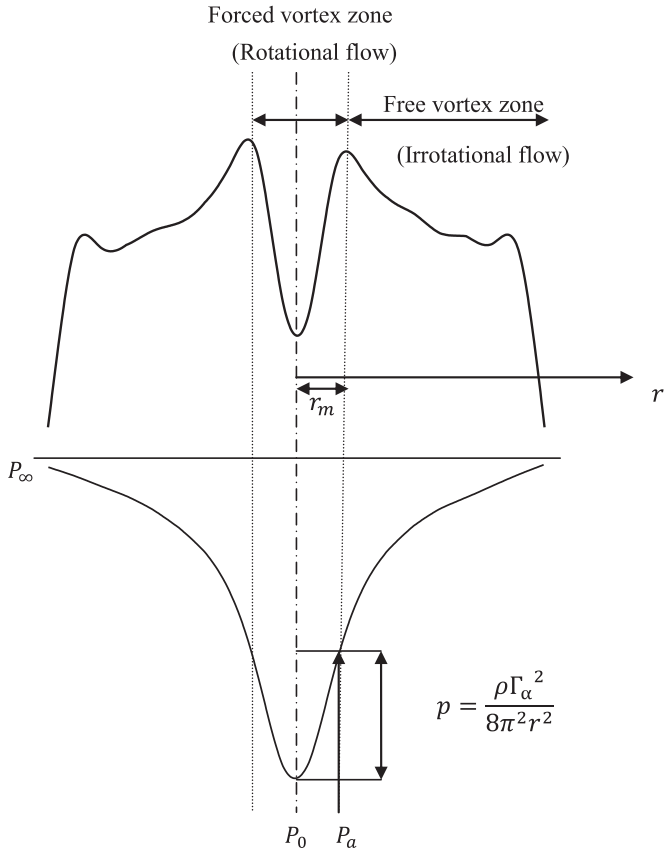

Fig. 11. Illustrative sketch of tangential velocity and pressure distributions in a Rankine vortex.

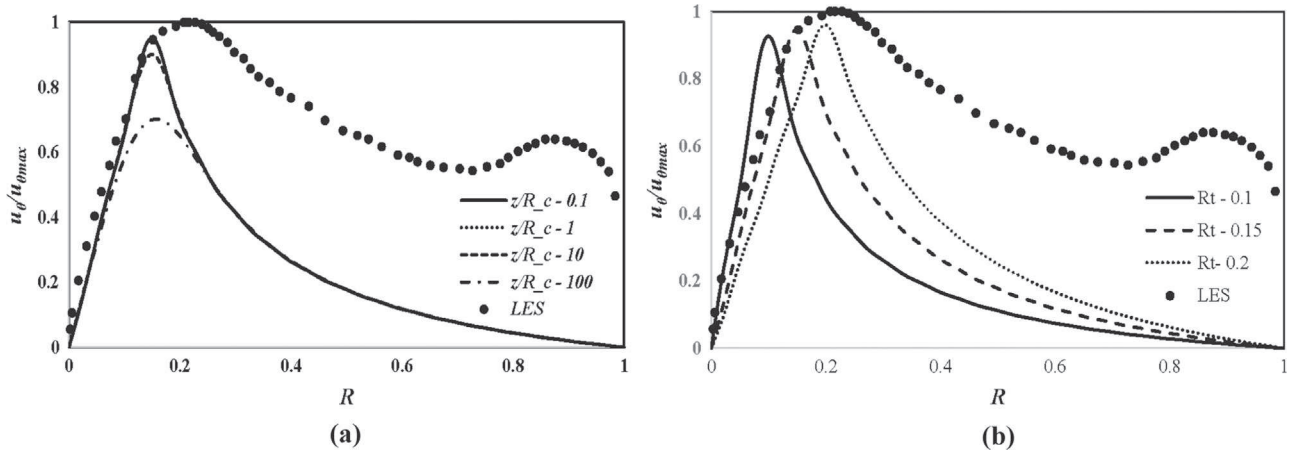

Fig. 12. Distribution of $u_\theta/u_{\theta max}$ with R (a) for different values of z/R_c and (b) for different values of R_t, as obtained from Eq. (9). The marker (●) shows the corresponding distribution of $u_\theta/u_{\theta max}$ corresponding to LES simulation.

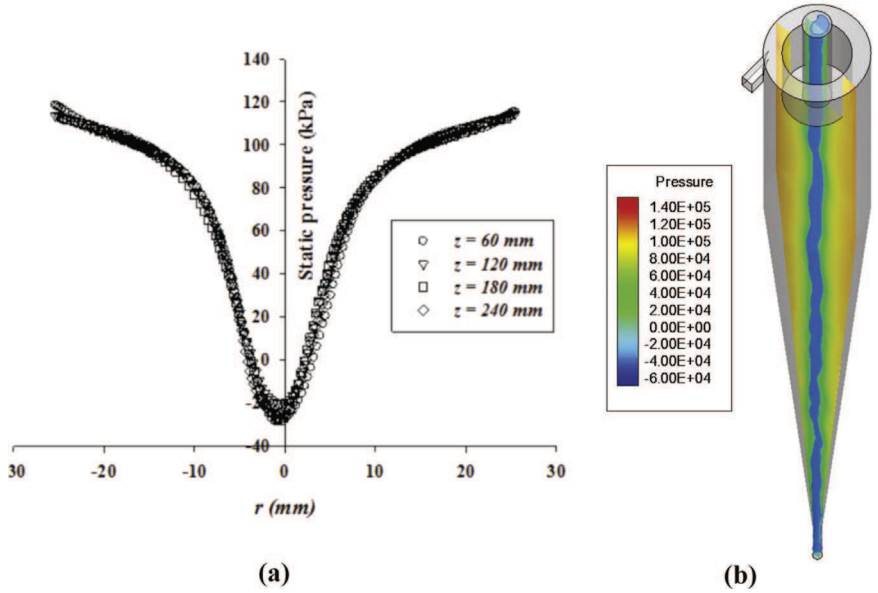

Fig. 13. (a) Distribution of static pressure as obtained from LES simulation and (b) contour plot of static pressure distribution along with isosurface of pressure core as obtained from single phase simulation. (For interpretation of the references to colour in this figure caption, the reader is referred to the web version of this paper.)

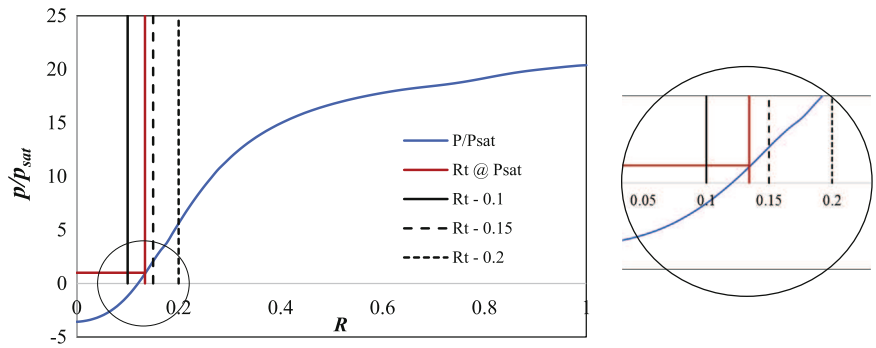

Fig. 14. (a) Distribution of p/p_{sat} as a function of R. Blue line is the distribution of p/p_{sat} as obtained from simulation. Red line denotes the air water interface boundary where $p = p_{sat}$. (For interpretation of the references to colour in this figure caption, the reader is referred to the web version of this paper.)

split mechanism, thereby establishing the correct flow field and pressure field. In the present study the numerical modelling has been confined to the single phase modelling, and the pressure distribution inside the hydrocyclone is used to determine the air core diameter. Fig. 13(a) represents the radial distribution of static pressure obtained through the numerical simulation along the different axial heights of the cyclone. The static pressure contour has been shown in Fig. 13(b). The blue shape zone at the centre represent the isosurface in which pressure is constant and equal to saturation vapour pressure of water. This isosurface represents the

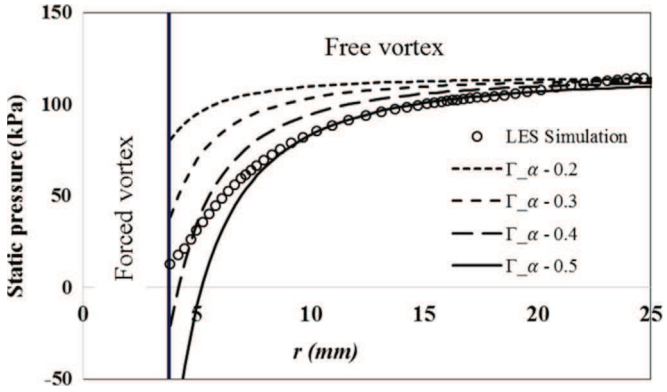

Fig. 15. Radial distribution of static pressure in free vortex region for the different values of Γ_α.

regions with the pressure below the saturation vapour pressure of water corresponding to the twisted depression of air core. In Fig. 14 we present the distribution of the p/p_{sat} with R, where p_{sat} is the saturation vapour pressure of water. In the figure red line indicates the air water interface where the static pressure is equal to saturation vapour pressure (i.e. $p/p_{sat} = 1$) resembling the air water interface. In general, for hydrocyclones the air core is mainly confined inside the forced vortex zone. However from this figure we also observe that at the radial location where R_t=0.15, static pressure is very close to the saturation pressure. From Eq. (12) it seems that $p_\infty - p_o$ varies as Γ_α^2 and $1/r^2$ as well. A plot of static pressure profiles at Γ_α = 0.2, 0.3, 0.4 and 0.5 is shown in Fig. 15, as obtained from using Eq. (12). Subsequently the radial distribution of static pressure profile from LES simulation has also been plotted in Fig. 15. This figure implies a governing role of Γ_α in pressure distribution in the free vortex region inside the hydrocyclone. The graphs are shown for R_t=0.15. From this figure it appears that Γ_α plays a significant role in deciding pressure profile in the free vortex region. This figure also implies a governing role of Γ_α in deciding the pressure drop between the free and the forced vortex region. The magnitude of G force is very much sensitive towards the pressure drop between the free and forced vortex region. From Fig. 16 we can observe that the pressure variation between the free and forced vortex region increases with the increase in P_{in}. It is imperative to note that as inlet pressure (or flow rate) increases the G force also increases at an identical radial location and the

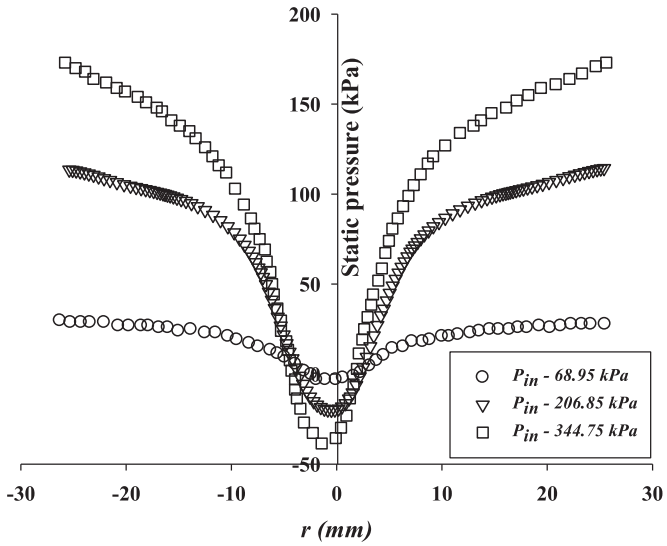

Fig. 16. Radial distribution of static pressure at different inlet pressures at same axial location.

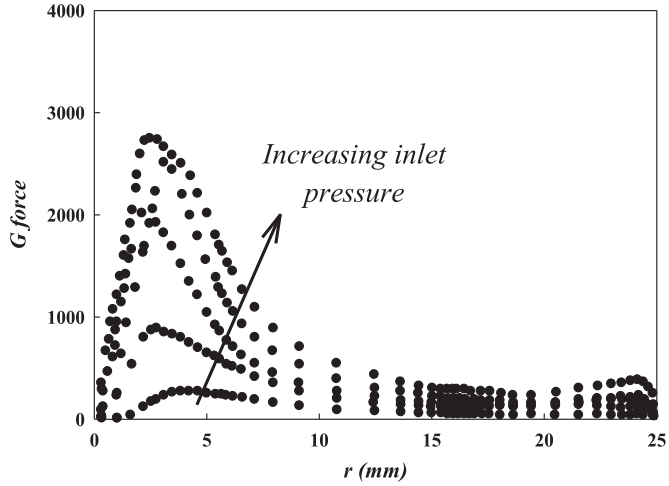

Fig. 17. Effect of inlet pressure ranging from 68.95 to 344.74 kPa on G force distribution.

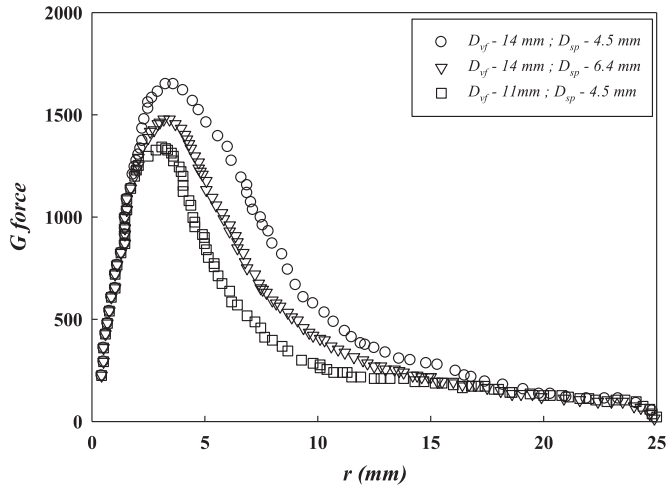

Fig. 18. Distribution of G force inside a hydrocyclone for different configurations of vortex finder and spigot.

effect is much more obvious near the location of forced vortex boundary. A sample plot of the changes in the G force distribution at different inlet pressures is shown in Fig. 17. As the fluid stream enters hydrocyclone through a tangential inlet, the velocity is converted into tangential velocity imparting a centrifugal force on the fluid. The separation is magnified since the ratio between the centrifugal force and the force of gravity is significantly greater in hydrocyclones. In view of the above perspective, it is essential to characterize the G force distribution inside the hydrocyclone and the consequences of G force on separation performance must be established in a quantitative way. In Fig. 18 the profiles for the radial distribution of G force for different cyclone configurations have been shown. It was shown in Fig. 13 at a given axial location a significant pressure drop was created along the radial direction which is probably attributed to the radial distribution of G force. This radial pressure drop probably causes a part of the flow to move towards the forced vortex region leading to a flow reversal. Again due to the flow fluctuations and the resultant decay in the swirling motion, G_{max} decreases along the axial location of the hydrocyclone from cylindrical section to conical section (see Fig. 9). Though the phenomenological characteristics of the flow behaviour we can say that the combined effect of G force variation along the radial as well as axial direction is the driving force for

flow split inside an operating hydrocyclone. Therefore in this paper the difference in magnitude of G force between the spigot and the cylindrical section, termed as G force differential (ΔG) has been proposed as a new hydrodynamic parameter for modelling the water partitioning behaviour. The estimation of G force for a fixed hydrocyclone geometry at a given operating condition can also be approximated (Bradly, 1965) from the following mathematical expression:

$$G = 2\alpha^2 \frac{V_i^2}{D_c g}\left(\frac{D_c}{d_c}\right)^{2n+1} \tag{13}$$

where α is a modifying factor for swirl losses approximated by $3.7(D_i/D_c)$ where D_i is the feed inlet diameter, D_c is the cyclone diameter, and g is the gravitational acceleration and n is a constant which normally varies between 0.5 and 0.8 (Bradly, 1965). V_i is the inlet velocity of the water and can be calculated by the following equation:

$$V_i = \frac{Q_i}{A_i} \tag{14}$$

where Q_i is the inlet volumetric flow rate and A_i is the cross sectional area of the feed inlet. The volumetric flow rate of water at each experimental condition can be calculated by adding the water flow rate through the underflow (Q_{if}) and the overflow (Q_{of}). Using Eq. (14) the values at the spigot and cylindrical regions of a hydrocyclone can be calculated easily and the difference between the calculated values, G at spigot and cylindrical region is termed as G force differential (ΔG).

3.1. Effect of inlet pressure on G force differential (ΔG)

We now discuss the dependency of ΔG on the inlet pressure, the vortex finder diameter and the spigot diameter. In Fig. 19, the variations of ΔG values with inlet pressure at different combinations of vortex finder diameters and spigot diameters have been illustrated. From this figure it may be observed that the ΔG value increases significantly with increasing inlet pressure at a fixed hydrocyclone geometry. It is also interesting to note that any change in either vortex finder diameter or spigot diameter also has significant impact on the ΔG value. This suggests that the separation performance in a hydrocyclone is mainly controlled by any parameter which affects the ΔG value. The performance of an industrial hydrocyclone is generally controlled by changing the spigot diameter keeping other variables unchanged. Any change in spigot diameter will, therefore, change the inlet flow rate for a fixed pressure inlet and will, therefore, have an impact on ΔG value.

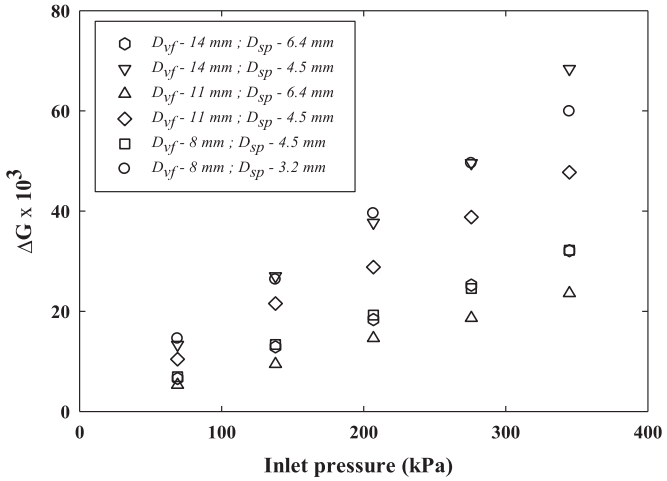

Fig. 19. Variation of G force difference with inlet flow rate for different hydrocyclone geometries, where D_{sp} is spigot diameter and D_{vf} is vortex finder diameter.

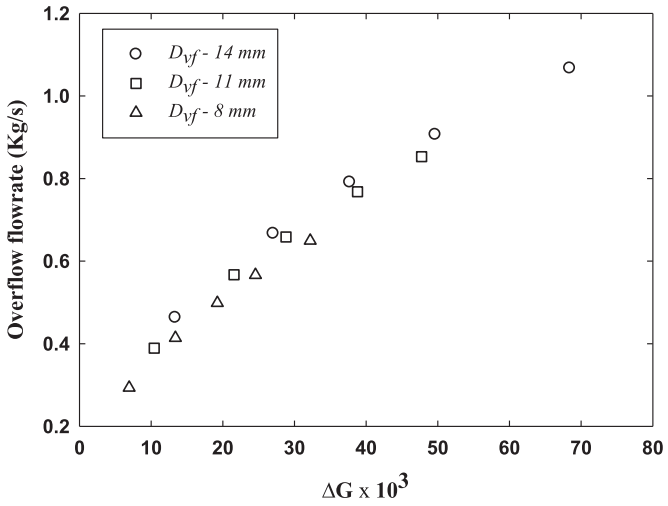

Fig. 20. Effect of G force difference on overflow flow rate, Q_{of} (kg/s).

3.2. Effect of G force differential (ΔG) on water split

To study the effect of ΔG on water recovery to overflow, the overflow mass flow rate (Q_{of}) has been plotted as a function of vortex finder diameters for a fixed spigot diameter (d_{sp} = 4.5 mm) as shown in Fig. 20. It is imperative from the above observation that with an increase in ΔG, the water recovery in overflow increases gradually. Actually the tangential entry of the fluid medium through the inlet at a high pressure imparts swirling motion to cause a significant variation in G force. The G force variation has a strong influence on the swirl flow transition from the forced to the free vortex zones which causes induced drag to drive the water through the periphery of the inner vortex to the overflow outlet. The quantity of this water to be transported through the vortex finder diameter will, therefore, depend on the intensity of this induced drag which is basically dependent on the ΔG created at that operating condition.

3.3. Effect of exit diameters on water split

It has been reported that for a given hydrocyclone there is an optimum range of vortex finder diameter below or above which the cyclone efficiency starts to decrease. From available literature it can be appreciated that increase in D_{vf}, keeping other variable constant, results in decrease in the separation efficiency of the hydrocyclone (Bradly, 1965; Wang and Yu, 2008; Ghodrat et al., 2014). This fact is often described by the subsequent decrease in G force. The optimum recommended vortex finder diameters are in the range of $D_c/3$–$D_c/6$ (Moder and Dahlstrom, 1952; Bradly, 1965). The dimensions of the vortex finders used in our present experiments were kept, therefore, within this range. The variation of water split with vortex finder diameter at various spigot diameters has been illustrated in Fig. 21. From the above plot it is observed that at a fixed spigot diameter (D_{sp}) along with a fixed inlet pressure the water recovery through overflow stream increases when vortex finder diameter D_{vf} increases. It is also evident from the figure that at a fixed D_{vf} and inlet pressure, the water recovery rate through overflow stream decreases when spigot diameter D_{sp} increases.

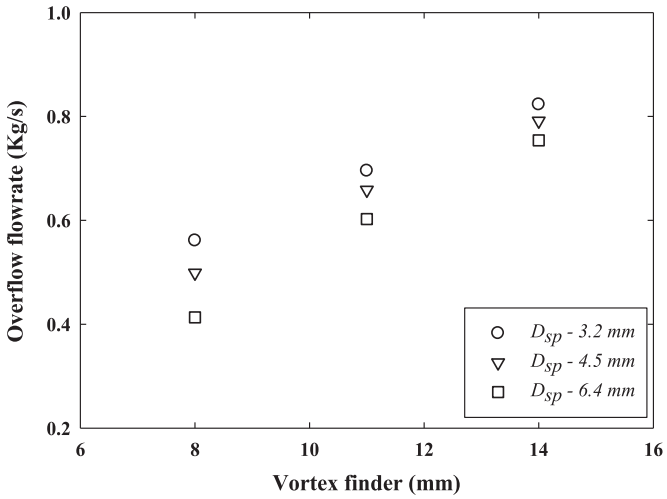

Fig. 21. Effect of vortex finder diameter on overflow flow rate, Q_{of} (kg/s).

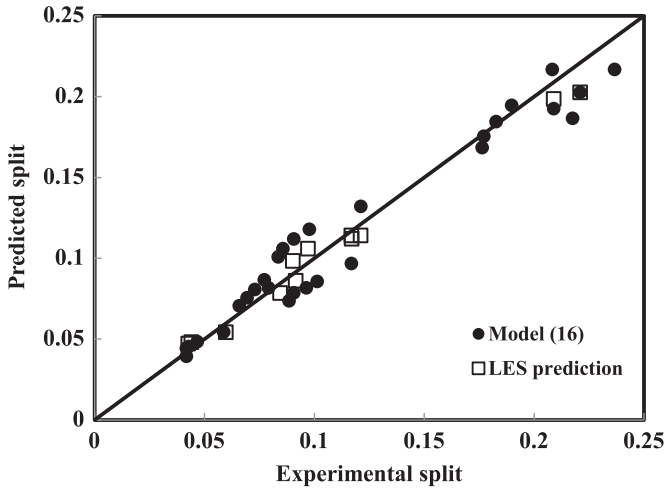

Fig. 22. Comparison between experimental and predicted water split.

4. Overall correlation and model validation

In order to interrelate the individual variables with water split (S) on the basis of above trend, an attempt has been made to derive an empirical correlation to quantify the combined effect of G force differential (ΔG) and cyclone design variables. Due to the formation of the inner core, the available cross sectional area for water to pass through cyclone overflow actually gets reduced significantly when the cyclones are under operation. Therefore, vortex finder diameter and spigot diameter have also been chosen as separate variables for the modelling purposes. The experimental data may, therefore, be expressed in the following form as

$$S = k(\Delta G)^{l}(D_{vf})^{m}(D_{sp})^{n} \tag{15}$$

To find the value of k and the exponents l, m and n respectively multiple regression analysis of all the experimental data were performed. Total number of 30 experiments were carried out within the range of the variables as given in Table 2.

The final form of the developed model becomes

$$S = 2.32(\Delta G)^{-0.17}(D_{vf})^{-2.34}(D_{sp})^{2.25} \tag{16}$$

The comparative plot between experimental water split and the predicted data is shown in Fig. 22. Here we also plotted the numerically computed water split data to quantify the competency of the develop model with the LES model. The predicted R^2 value (0.953), being very close to the adjusted R^2 (0.947), signifies that the model is in good agreement with the experimentally observed trends of data. The statistical data for the model are shown in Table 3. The above statistical analysis confirms the significance of the p values which justifies the fact that the model parameters are adequate to fit in the regression model to compute the observed trend of the experimental data.

Table 3
Evaluation of the statistical analysis of the regression model.

Parameter	Coefficient	p
D_{vf}	−2.34	<0.001
D_{sp}	2.25	<0.001
ΔG	0.17	0.001

5. Conclusions

Water partitioning mechanism in a hydrocyclone is explained in this paper based on numerical analysis of the flow field analysis using large eddy simulations (LES) technique. It has been shown that the complex pattern of vortex flow in a hydrocyclone has similarity with Rankine vortex type flow. A new hydrodynamic parameter, termed as G force differential or ΔG, has been proposed in this paper which essentially helps in quantifying the pressure drop between the spigot and the vortex finder region. Any change in operating and design variables of hydrocyclone actually changes the nature of the swirling flow patterns which ultimately affects ΔG. Systematic experimental data were also generated in a 50.8 mm diameter hydrocyclone to observe the variation of the water split with ΔG and other design parameters. With the support of numerical understanding of the convoluted hydrodynamics, a semi-empirical model has been developed to compute the water split inside a hydrocyclone in a quantifiable manner. The developed model shows a reasonable agreement with the experimental observations and LES predictions as well. Therefore, it can be concluded that the proposed hydrodynamic parameter ΔG actually causes the flow split and can be used as a scaling parameter in order to compute the performance of hydrocyclones. However, at the end, it needs to mention that detailed analysis of particle classification pattern inside a hydrocyclone with the framework of present modelling approach is preserved as a scope of future research.

Table 2
Data set used for model development.

Hydrocyclone	Diameter (mm)	Vortex finder (mm)	Spigot (mm)	Inlet pressure (kPa)
1	50.8	14	6.4	68.95, 137.90, 206.84, 275.79, 344.74
2	50.8	14	4.5	68.95, 137.90, 206.84, 275.79, 344.74
3	50.8	11	6.4	68.95, 137.90, 206.84, 275.79, 344.74
4	50.8	11	4.5	68.95, 137.90, 206.84, 275.79, 344.74
5	50.8	8	3.2	68.95, 137.90, 206.84, 275.79, 344.74
6	50.8	8	4.5	68.95, 137.90, 206.84, 275.79, 344.74

References

Abbot, J., 1962. Cyclone circuits. Trans. Inst. Miner. Metall. 71.

Banerjee, C., Chaudhury, K., Majumder, A.K., Chakraborty, S., 2015. Swirling flow hydrodynamics in hydrocyclone. Ind. Eng. Chem. Res. 54 (1), 522–528.

Bradly, D., 1965. The Hydrocyclones, 4th ed. Pergamon Press, London.

Brennan, M., 2006. CFD simulations of hydrocyclones with an air core: comparison between large eddy simulations and a second moment closure. Chem. Eng. Res. Des. 84 (6), 495–505.

Chen, W., Zydek, N., Parma, F., 2000. Evaluation of hydrocyclone models for practical applications. Chem. Eng. J. 80 (1), 295–303.

Chu, L.-Y., Yu, W., Wang, G.-J., Zhou, X.-T., Chen, W.-M., Dai, G.-Q., 2004. Enhancement of hydrocyclone separation performance by eliminating the air core. Chem. Eng. Process.: Process Intensif. 43 (12), 1441–1448.

Coelho, M., Medronho, R., 2001. A model for performance prediction of hydrocyclones. Chem. Eng. J. 84 (1), 7–14.

Dabir, B., Petty, C., 1984. Laser Doppler anemometry measurements of tangential an axial velocity in a hydrocyclone operating without an air core. In: Second International Conference on Hydrocyclones, England, pp. 15–40.

Darmofal, D., Khan, R., Greitzer, E., Tan, C., 2001. Vortex core behaviour in confined and unconfined geometries: a quasi-one-dimensional model. J. Fluid Mech. 449, 61–84.

Davailles, A., Climent, E., Bourgeois, F., 2012. Fundamental understanding of swirling flow pattern in hydrocyclones. Sep. Purif. Technol. 92, 152–160.

Delgadillo, J.A., Rajamani, R.K., 2007. Exploration of hydrocyclone designs using computational fluid dynamics. Int. J. Miner. Process. 84 (1), 252–261.

Delgadillo, J.A., Rajamani, R.K., 2009. Computational fluid dynamics prediction of the air-core in hydrocyclones. Int. J. Comput. Fluid Dyn. 23 (2), 189–197.

Evans, W.K., Suksangpanomrung, A., Nowakowski, A.F., 2008. The simulation of the flow within a hydrocyclone operating with an air core and with an inserted metal rod. Chem. Eng. J. 143 (1), 51–61.

Fisher, M., Flack, R., 2002. Velocity distributions in a hydrocyclone separator. Exp. Fluids 32 (3), 302–312.

Ghodrat, M., Kuang, S., Yu, A., Vince, A., Barnett, G., Barnett, P., 2014. Numerical analysis of hydrocyclones with different vortex finder configurations. Miner. Eng. 63, 125–138.

Gupta, R., Kaulaskar, M., Kumar, V., Sripriya, R., Meikap, B., Chakraborty, S., 2008. Studies on the understanding mechanism of air core and vortex formation in a hydrocyclone. Chem. Eng. J. 144 (2), 153–166.

Hsieh, K., Rajamani, R., 1991. Mathematical model of the hydrocyclone based on physics of fluid flow. AIChE J. 37 (5), 735–746.

Hwang, K.-J., Hwang, Y.-W., Yoshida, H., 2013. Design of novel hydrocyclone for improving fine particle separation using computational fluid dynamics. Chem. Eng. Sci. 85, 62–68.

Hwang, K.-J., Hwang, Y.-W., Yoshida, H., Shigemori, K., 2012. Improvement of particle separation efficiency by installing conical top-plate in hydrocyclone. Powder Technol. 232, 41–48.

Julien, P., 1986. Concentration of very fine silts in a steady vortex. J. Hydraul. Res. 24 (4), 255–264.

Karimi, M., Akdogan, G., Dellimore, K., Bradshaw, S., 2012. Quantification of numerical uncertainty in computational fluid dynamics modelling of hydrocyclones. Comput. Chem. Eng. 43, 45–54.

Kelsall, D., 1952. A Study of the Motion of Solid Particles in a Hydraulic Cyclone. Technical Report. Atomic Energy Research Establishment, Harwell, Berks, England.

Knowles, S.R., Woods, D.R., Feuerstein, I.A., 1973. The velocity distribution within a hydrocyclone operating without an air core. Can. J. Chem. Eng. 51 (3), 263–271.

Kolmogorov, A., 1941. The local structure of turbulence in incompressible viscous fluids at very large Reynolds numbers. Proc. R. Soc. 434, 9–13.

Kreith, F., Sonju, O., 1965. The decay of a turbulent swirl in a pipe. J. Fluid Mech. 22 (02), 257–271.

Lim, E.W.C., Chen, Y.-R., Wang, C.-H., Wu, R.-M., 2010. Experimental and computational studies of multiphase hydrodynamics in a hydrocyclone separator system. Chem. Eng. Sci. 65 (24), 6415–6424.

Lynch, A., Rao, T., 1975. Modeling and scaling up of hydrocyclone classifiers. In: Proceedings of the 11th International Mineral Processing Congress, pp. 245–270.

Mainza, A., Narasimha, M., Powell, M., Holtham, P., Brennan, M., 2006. Study of flow behaviour in a three-product cyclone using computational fluid dynamics. Miner. Eng. 19 (10), 1048–1058.

Moder, J., Dahlstrom, D., 1952. Fine-size, close-specific-gravity solid separation with the liquid–solid cyclone. Chem. Eng. Prog. 48 (2), 75–88.

Murthy, Y.R., Bhaskar, K.U., 2012. Parametric CFD studies on hydrocyclone. Powder Technol. 230, 36–47.

Nageswararao, K., Wiseman, D., Napier-Munn, T., 2004. Two empirical hydrocyclone models revisited. Miner. Eng. 17 (5), 671–687.

Narasimha, M., Brennan, M., Holtham, P., 2006. Large eddy simulation of hydrocyclone prediction of air-core diameter and shape. Int. J. Miner. Process. 80 (1), 1–14.

Narasimha, M., Mainza, A., Holtham, P.N., Powell, M., Brennan, M.S., 2014. A semi-mechanistic model of hydrocyclones developed from industrial data and inputs from CFD. Int. J. Miner. Process. 133, 1–12.

Ovalle, E., Concha, F., 2005. The role of wave propagation in hydrocyclone operations. II: wave propagation in the air-water interface of a conical hydrocyclone. Chem. Eng. J. 111 (2), 213–223.

Pericleous, K.A., Rhodes, N., Cutting, G., 1984. A mathematical model for predicting the flow field in a hydrocyclone classifier. In: Second International Conference on Hydrocyclone, Bath, England, pp. 27–38.

Plitt, L., 1976. A mathematical model of the hydrocyclone classifier. CIM Bull. 69 (776), 114–123.

Plitt, L., Conil, P., Broussaud, A., 1990. An improved method of calculating the water-split in hydrocyclones. Miner. Eng. 3 (5), 533–535.

Shah, H., Majumder, A., Barnwal, J., 2006. Development of water split model for a 76 mm hydrocyclone. Miner. Eng. 19 (1), 102–104.

Slack, M., Prasad, R., Bakker, A., Boysan, F., 2000. Advances in cyclone modelling using unstructured grids. Chem. Eng. Res. Des. 78 (8), 1098–1104.

Sripriya, R., Kaulaskar, M., Chakraborty, S., Meikap, B., 2007. Studies on the performance of a hydrocyclone and modeling for flow characterization in presence and absence of air core. Chem. Eng. Sci. 62 (22), 6391–6402.

Swain, S., Mohanty, S., 2013. A 3-dimensional Eulerian–Eulerian CFD simulation of a hydrocyclone. Appl. Math. Model. 37 (5), 2921–2932.

Wang, B., Chu, K., Yu, A., 2007. Numerical study of particle–fluid flow in a hydrocyclone. Ind. Eng. Chem. Res. 46 (13), 4695–4705.

Wang, B., Yu, A., 2008. Numerical study of the gas–liquid–solid flow in hydrocyclones with different configuration of vortex finder. Chem. Eng. J. 135 (1), 33–42.

Yao, S., Fang, T., 2012. Analytical solutions of laminar swirl decay in a straight pipe. Commun. Nonlinear Sci. Numer. Simul. 17 (8), 3235–3246.

Yoshioka, N., Hotta, Y., 1955. Liquid cyclone as a hydraulic classifier. Chem. Eng. Jpn. 19 (12), 632–640.

Zhen-Bo, W., Yi, M., You-Hai, J., 2011. Simulation and experiment of flow field in axial-flow hydrocyclone. Chem. Eng. Res. Des. 89 (6), 603–610.

Zhu, G., Liow, J.-L., Neely, A., 2012. Computational study of the flow characteristics and separation efficiency in a mini-hydrocyclone. Chem. Eng. Res. Des. 90 (12), 2135–2147.